Bound Site of Mo Atoms and Its Local Structure in a Mo/HY Catalyst Characterized by Extended X-ray Absorption Fine Structure and Density Functional Calculation†

Takehiko Sasaki,‡ Fusao Nakagawa,§ and Yasuhiro Iwasawa*,§

Department of Complexity Science and Engineering, Graduate School of Frontier Sciences, The University of Tokyo, 5-1-5 Kashiwanoha, Kashiwa, Chiba 277-8561, Japan, and Department of Chemistry, Graduate School of Science, The University of Tokyo, Hongo, Bunkyo-ku, Tokyo 113-0033, Japan

Received: March 1, 2004; In Final Form: May 17, 2004

The bound site of Mo atoms and its local structure in a Mo/HY catalyst have been determined by detailed analysis of extended X-ray absorption fine structure (EXAFS). Molybdenum was introduced in the supercage of HY zeolite by cycles of saturated adsorption of $Mo(CO)_6$ at room temperature and subsequent thermal decomposition at 573 K. Two Mo atoms per supercage were immobilized in each CVD-thermal treatment cycle. The Mo loading increased linearly with the cycles up to three cycles at saturation, where six Mo atoms were supported. Temperature-programmed decomposition of the adsorbed $Mo(CO)_6$ was also characterized by GC, QMS, and FT-IR, respectively. The EXAFS analysis including multiple scattering based on theoretical calculations revealed that Mo bound with two oxygen atoms connects to Al, where one of the two oxygen atoms had been associated with a proton. The bound site is called the S_{III}' site. The zeolite framework was significantly distorted by the introduction of low-valent Mo, resulting in isolation of the $[MoO_2Al]$ unit from the surrounding zeolite framework due to a quasi-disruption of Si−O bonds adjacent to the unit. In the mild oxidation of the low-valent Mo/HY sample two Mo═O bonds were newly formed and the position of Mo was displaced by 0.06 nm so that the distortion of zeolite framework around the Al atom was relieved. The structures were also supported by DFT calculations. This study is the first example that the position of metal cation in zeolite was determined unambiguously by the EXAFS analysis.

Introduction

Activity and selectivity are key issues to be addressed for catalysis. These issues should be related to structure and location of active sites in heterogeneous catalysts, but it is generally difficult to obtain these structural information at an atomic/molecular level. In this context, preparation of well-defined catalysts with definite structures has been extensively studied to allow discussion on structure−performance correlation and molecular-level mechanism.[1−3]

Zeolites as crystalline microporous materials provide nanospaces for syntheses of active catalytic materials,[4] in which nanosized metal clusters and particles, organometallic complexes, and so on have been designed by using suitable precursors.[5−10] Encapsulation of Mo species in zeolites has received much attention because Mo is an active element such as selective oxidation, hydrogenation, metathesis, hydrodesulfurization, hydrodenitrogenation, and so on. $Mo(CO)_6$ is a convenient source to prepare Mo catalysts by a CVD method followed by the decarbonylation process. The decarbonylation processes of $Mo(CO)_6$ in Y zeolites have been characterized by FT-IR,[11−15] extended X-ray absorption fine structure (EXAFS),[16,17] energy-dispersive XAFS (DXAFS),[18,19] temperature-programmed desorption (TPD),[20,21] and electron-spin resonance (ESR).[22] Okamoto et al. suggested that $Mo(CO)_3(O_L)_3$ (O_L, oxygen atoms of the zeolite framework) in NaY zeolite was formed by the decarbonylation of $Mo(CO)_6$/NaY at 373 K.[17] Asakura et al. revealed that Mo(II) oxocarbidic dimer species $Mo_2(C)O_x$ was formed in NaY zeolite at 573 K. The produced $Mo_2(C)O_x$ species in NaY supercages showed a unique catalytic property for methanol reaction.[23] The decarbonylation process of $Mo(CO)_6$/HY was studied by Abdo and Howe,[13,22] who observed H_2 evolution during the decarbonylation and indicated that the Mo(0) species was oxidized by a proton to form the Mo(I) species. Yamaguchi et al. studied the decarbonylation processes of $Mo(CO)_6$ in NaY and HY by time-resolved DXAFS and detected unstable intermediate structures.[18,19]

In structural characterization of zeolite-supported catalysts the location of incorporated metal cations is also an important issue relevant to the catalytic performance. Figure 1 shows cationic sites determined for Faujasite type zeolites. EXAFS allows us to analyze the local structure around metal cations and their location in zeolites. This study reports the first example of the detailed EXAFS analysis including multiple scattering for the location and structure of Mo cations in HY zeolite.

Experimental Section

Catalyst Preparation. HY zeolite (Si/Al = 2.8) was supplied from Toso Co. (HSZ-320HOA). The HY sample involves 4 wt % as Na_2O, the BET surface area is 550 $m^2\ g^{-1}$, and the crystal size is 0.3 μm. $Mo(CO)_6$ was purchased from Soekawa Chemicals Co. and used without further purification. The zeolite was pretreated under vacuum (10^{-3} Pa) at 723 K for 15 min and calcined at the same temperature under 26.6 kPa of oxygen for 30 min, followed by evacuation at 723 K for 1 h in a closed

† Part of the special issue "Michel Boudart Festschrift".

* Corresponding author. Fax: +81-3-5800-6892. E-mail: iwasawa@chem.s.u-tokyo.ac.jp.

‡ Department of Complexity Science and Engineering.

§ Department of Chemistry.

10.1021/jp049090a CCC: $30.25
Published on Web 06/25/2004

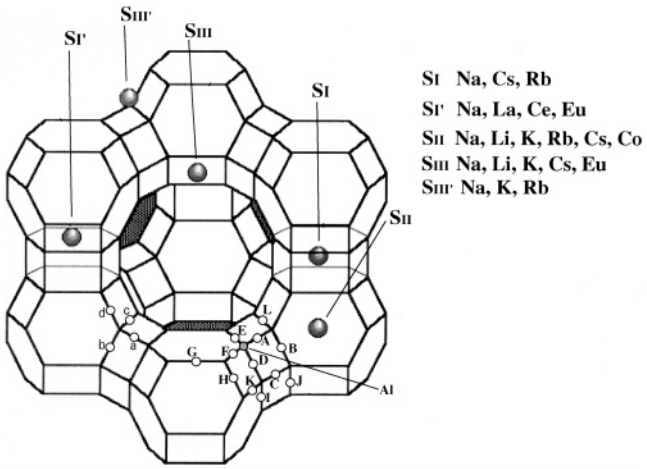

Figure 1. Representation of sodalite cage, hexagonal prism in the framework of faujasite type zeolite. Sites for cations, S_I, S_I', S_{II}, S_{III}, and S_{III}' are indicated and the reported cations for each site are listed.

circulating system. The treated zeolite was then saturated with $Mo(CO)_6$ by exposing $Mo(CO)_6$ vapor at room temperature for 15 h. This sample is denoted as $Mo(CO)_6$/HY hereinafter. Decarbonylation of $Mo(CO)_6$/HY was achieved by annealing it to 573 K at a heating rate of 10 K min^{-1} under vacuum and maintaining the temperature for 1 h. The sample obtained by a cycle of the $Mo(CO)_6$ adsorption and the decarbonylation is denoted as Mo(1)/HY. The processes of the saturated adsorption of $Mo(CO)_6$ and the thermal treatment under vacuum at 573 K were repeated several times to obtain samples with various Mo loadings. The samples thus obtained are denoted as Mo(*n*)/HY, where *n* indicates the number of adsorption-thermal decomposition cycles.

X-ray Fluorescence. X-ray fluorescence (XRF) was measured on a JSX-3220 spectrometer (SEIKO Instruments Inc.) using a Rh target. Physical mixtures of MoO_3 and pretreated HY in various ratios were used as references to estimate the loadings of Mo in the samples.

FT-IR. Fourier transform infrared (FT-IR) spectra in a transmission mode (self-supported wafer) were measured to estimate residual hydroxyl groups of HY without exposure to air using a JIR-7000 spectrometer (JEOL Co.) with a resolution of 2 cm^{-1} and the repetition number of 200.

EXAFS Analysis. EXAFS spectra were measured at BL-10B of the Photon Factory in the Institute of Materials Structure Science, High Energy Accelerator Research Organization (KEK-MSS-PF). The electron storage ring was operated at 2.5 GeV and 300−400 mA. Synchrotron radiation from the storage ring was monochromatized by a Si(311) channel cut crystal. An ionization chamber filled with $Ar-N_2 = 1:1$ mixed gas with a path length of 17 cm was used as the detector monitoring incident X-ray (I_0) and the one with pure Ar with a path length of 31 cm × 2 was used for monitoring transmitted X-ray (I). The angle of the monochromator was calibrated by using a Mo foil, setting the inflection point at the absorption edge as 20 004 eV. The samples were mixed with BN (Wako Pure Chemicals Industries Co.) so that $\Delta\mu t$ became equal to 1.

The EXAFS spectra measured at room temperature were analyzed by the UWXAFS package.[24] The threshold energy E_0 was tentatively set at the inflection point of the absorption edge. The background was subtracted by using the AUTOBK program. The k^3-weighted EXAFS data were Fourier transformed into *R* space. The curve-fitting analysis was carried out using the FEFFIT program in the *R* space. The *k* range for the Fourier transformation and the fitting *R* range were 30−120 nm^{-1} and 0.10−0.42 nm, respectively. The number of independent parameters (N_{ind}) in the curve fitting for Mo/HY was evaluated to be 20.3 from the Nyquist law,[25] $N_{ind} = 2\Delta k\Delta R/\pi + 2$. Therefore the maximum number of parameters available for the fitting is 19. The fitting parameters were coordination numbers (CN), interatomic distances (*R*), Debye−Waller factors (σ), and a correction of edge energy (ΔE_0). The same ΔE_0 was used for all shells in a sample. The amplitude reduction factor S_0^2 was estimated using reference compounds. The phase shift and backscattering amplitude were calculated by the FEFF 8.00 code.[26]

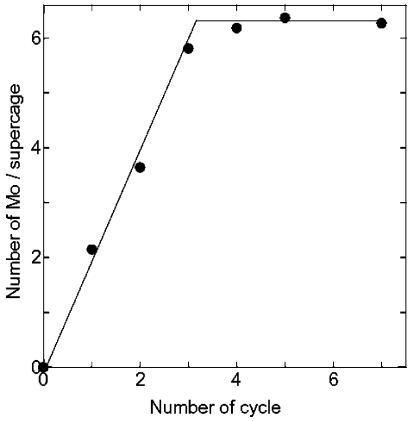

Figure 2. Number of Mo deposited per supercage as a function of the number of the saturated adsorption/thermal decomposition cycle.

TPD. Temperature-programmed decomposition (TPD) experiments were carried out in a closed circulating system at a ramping rate of 2 K min^{-1}. The evolved gases in the TPD process were analyzed by a quadrupole mass spectrometer for qualitative analysis and a gas chromatograph for quantitative analysis.

DFT Calculation. Density functional theory (DFT) calculations were performed using Dmol3 4.2.1[27] (Accelrys, USA). In all the calculations, spin−orbitals were restricted. The numerical basis set DNP was adopted, which is of double-ζ plus polarization functions quality. The orbitals included in the calculations were 1s and 2s for hydrogen, 1s, 2s, 2p, and 3d for oxygen atoms, 1s, 2s, 2p, 3s, 3p, and 3d for silicon and aluminum atoms, and 4s, 4p, 4d, 5s, and 5p for molybdenum atom. The criteria for the convergence of electronic states was 1.0×10^{-5} for the rms change in the norm of the electron density matrix. For the exchange-correlation functional, the nonlocal general gradient approximation given by Perdew and Wang was used through all the SCF (self-consistent field) cycles.[28] Structural optimization was performed by the DIIS (direct inversion in the iterative subspace) algorithm and the criteria for convergence was 0.05 kcal mol^{-1} in this study.

Results

Amount of Encapusulated $Mo(CO)_6$. Figure 2 shows the amount of $Mo(CO)_6$ encapsulated in a supercage of HY zeolite measured by XRF against the number of cycles for CVD and decarbonylation. The ordinate represents the number of Mo atoms per supercage of HY zeolite. Two Mo atoms in a supercage were supported by one cycle in agreement with our previous study[16] using a NaY zeolite. This result is reasonable because the diameter of the supercage of Y zeolite is about 1.2 nm and the size of $Mo(CO)_6$ is about 0.6 nm. Up to three cycles each cycle resulted in the introduction of two Mo atoms per a supercage and after four cycles the adsorption of $Mo(CO)_6$ did

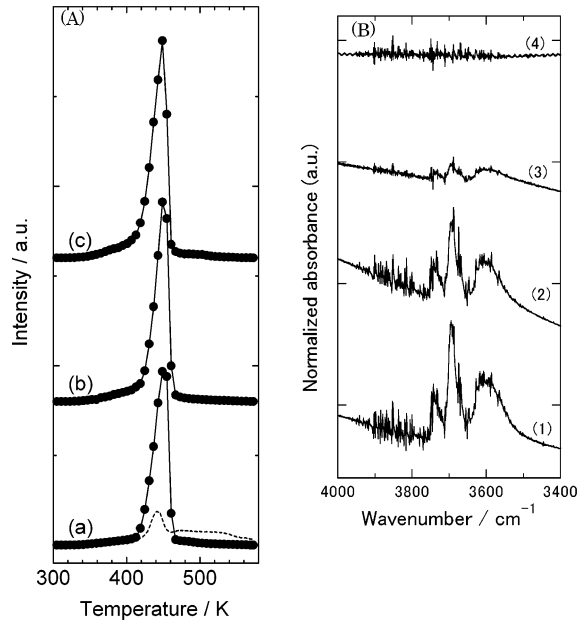

Figure 3. (A) Temperature-programmed decomposition spectra (TPD) for $Mo(CO)_6$ adsorbed on HY: (a) Mo/HY 1 cycle, (b) Mo/HY 2 cycles, and (c) Mo/HY 3 cycles, obtained by GC. H_2 evolution detected by MS is also shown for the Mo/HY 1 cycle sample as a broken line. Heating rate: 2 K min^{-1}. (B) FT-IR spectra obtained for (1) HY, (2) Mo/HY 1 cycle, (3) Mo/HY 2 cycles, and (4) Mo/HY 3 cycles.

not occur any more, indicating that the saturated Mo quantity in a supercage is six atoms. This result is in contrast to eight Mo atoms in a NaY supercage.[16] The linear increase in the Mo encapsulation and the definite break at the saturated Mo quantity, which are geometrically reasonable, indicate almost uniform encapsulation of Mo species in the HY supercages.

TPD spectra for $Mo(CO)_6$/HY were measured by a mass spectrometer, as shown in Figure 3A. The thermal decomposition of $Mo(CO)_6$ in HY takes place at 450 K, which is lower than 475 K for $Mo(CO)_6$/NaY.[16] Because two $Mo(CO)_6$ molecules adsorb in a supercage every cycle, 12 CO molecules are expected to desorb in one cycle. The amounts of desorbed CO were 8.8, 10.5, and 11.1 for the first, second, and third processes, respectively. The values are smaller than 12. After each sampling in a closed system for GC analysis, the gas phase was evacuated for 5 s. The loss of CO was accumulated in the repeated sampling, leading to CO amounts smaller than 12. There is also a possibility that all of the produced CO in the TPD experiments in a closed system are not measured by a mass spectrometer because of adsorption of the part of CO by the HY zeolite, particularly in the first run. Further, a small amount of CO_2 may be formed in the TPD process, which also gives a CO value smaller than 12. Anyhow, no CO evolution was observed during the $Mo(CO)_6$ adsorption in HY at room temperature, indicating no decomposition of $Mo(CO)_6$ in HY at room temperature. Judging from the shape of the desorption curve, the desorption of CO is of first order, supporting that this process is the simple thermal decomposition of $Mo(CO)_6$. Almost the same peak position in the TPD spectra for the 1−3 cycles indicates nearly uniform character of $Mo(CO)_6$ in the HY supercages.

FT-IR Measurements. Desorption of CO is accompanied by H_2 evolution, which indicates that protons (OH group) react with the Mo species, resulting in the chemical attachment of Mo atoms on the wall of supercages. This is confirmed by FT-IR spectra in Figure 3B. All the spectra were normalized with respect to the intensity of Al−O stretching mode at 1800−2000 cm^{-1}. The intensity of O−H stretching peaks was less intense after the CVD- decarbonylation process in comparison with the pretreated HY zeolite. The O−H stretching peak further reduced with subsequent cycles and almost diminished after the third cycle.

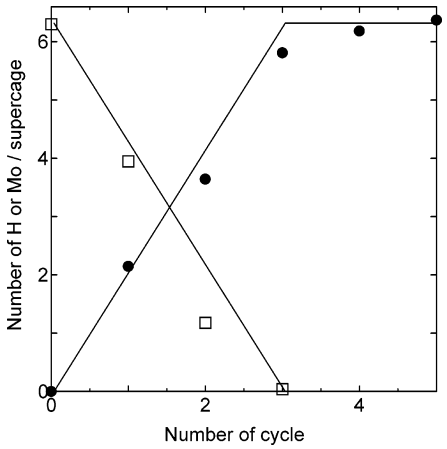

Figure 4. Number of Mo (filled circle) and H atoms (square) per supercage as a function of the number of the saturated adsorption/thermal decomposition cycle.

Figure 4 shows the amounts of H per a supercage versus the number of CVD cycles. Because the Si/Al ratio of HY zeolite used in this study is 2.8, 6.3 protons exist in a supercage before the CVD. The intensity of the O−H stretching peak was assumed to be proportional to the amount of OH groups. Figure 4 also shows the relation between the amount of Mo per supercage and the CVD cycles in Figure 2. These two traces in Figure 4 demonstrate that one proton is consumed by the reaction with one Mo atom. H_2 evolution in TPD typically as shown in Figure 3A(a)(broken line) was approximately quantitative to the Mo amount (Mo:H = 1:1) though the H_2 analysis by mass signal includes a large error. These results agree with the ESR data reported by Abdo and Howe, which revealed that thermal decomposition of $Mo(CO)_6$ in HY initially resulted in Mo^+ species.[22]

Mo K-Edge EXAFS. Mo K-edge EXAFS spectra were measured to investigate the local structure around Mo. The analyses of Mo reference compounds were performed to determine a many-body amplitude-reduction factor S_0^2. Table 1 lists the curve fitting results. S_0^2 ranged from 0.8 to 0.9 for Mo foil, $Mo(CO)_6$, $Mo_2(CH_3COO)_4$, and Na_2MoO_4, as shown in Table 1. Therefore, S_0^2 was set to be 0.85 in this study. Figure 5 shows k^3-weighted EXAFS oscillations and Fourier transforms for the Mo(1)/HY, Mo(2)/HY, and Mo(3)/HY samples. The EXAFS data for a Mo(1)/HY sample oxidized under a mild oxidation condition are also shown in Figure 5. Mo(1)/HY in a Schlenk tube was dipped in liquid nitrogen and 1 equiv of oxygen with respect to Mo was admitted in the tube, where all oxygen was adsorbed, showing zero pressure. After the tube was heated to room temperature, 0.08 molecule of oxygen with respect to Mo was consumed after 1 h. After annealing to 573 K, it was found that 0.8 molecule of O_2 with respect to Mo was consumed. In this mild oxidation condition the framework of the HY zeolite was retained, as proved by XRD (not shown).

The EXAFS data for Mo(n)/HY (n = 1−3) show a similar feature independent of the number of CVD−decarbonylation cycles, indicating that the local structures around Mo are the same for these samples with different Mo loadings. It is to be noted that a small peak near 0.4 nm appeared in the FT spectra. Normal curve fitting was performed for these spectra. The coordination number for the nearest neighbor Mo−O shell was

TABLE 1: Curve Fitting Results of Mo K-Edge EXAFS Data for Reference Samples[a]

sample	shell	CN	R/0.1 nm	$\sigma/10^{-4}$ nm	ΔE_0/eV	S_0^2	R_f/%
Mo foil	Mo−Mo	8 (fix)	2.73 ± 0.01	4.1 ± 0.4	1.1 ± 0.6	0.90 ± 0.06	0.06
	Mo−Mo	6 (fix)	3.15 ± 0.01	3.7 ± 0.6			
$Mo(CO)_6$	Mo−C	6 (fix)	2.07 ± 0.01	2.3 ± 0.9	2.3 ± 0.9	0.85 ± 0.09	1.48
	Mo−O	6 (fix)	3.22 ± 0.01	3.8 ± 0.9			
	Mo−(C)−O	12 (fix)	3.22 ± 0.01	3.8 ± 0.9			
	Mo=C=O	6 (fix)	3.22 ± 0.01	3.8 ± 0.9			
$Mo_2(CH_3CO_2)_4$	Mo−Mo	1 (fix)	2.10 ± 0.02	1 ± 2	4 ± 4	0.8 ± 0.3	3.04
	Mo−O	4 (fix)	2.14 ± 0.03	4 ± 5			
Na_2MoO_4	Mo−O	4 (fix)	1.79 ± 0.01	1.6 ± 0.4	1 ± 1	0.82 ± 0.05	0.22

[a] Fitting ranges of each reference compound are (a) 0.20−0.30 nm for Mo foil, (b) 0.10−0.30 nm for $Mo(CO)_6$, (c) 0.10−0.23 nm for $Mo_2(CH_3CO_2)_4$, and (d) 0.10−0.20 nm for Na_2MoO_4.

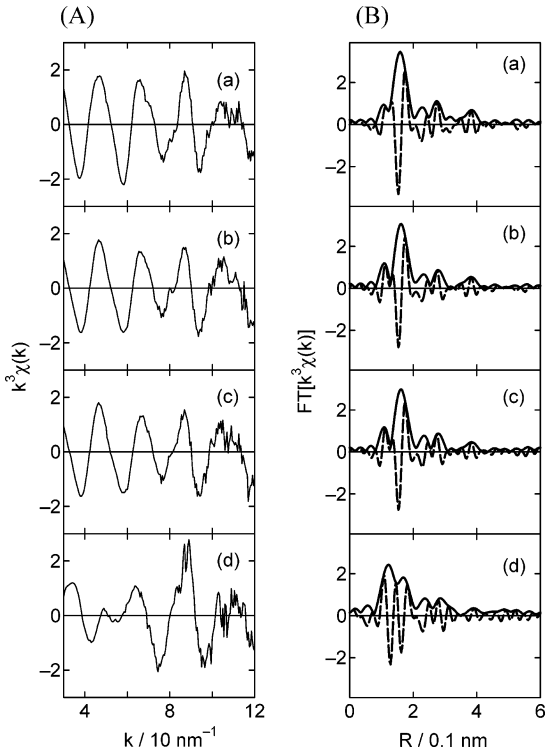

Figure 5. k^3-weighted EXAFS oscillations (A) and Fourier transforms (B) of (a) Mo/HY 1 cycle, (b) Mo/HY 2 cycles, (c) Mo/HY 3 cycles, and (d) Mo/HY 1 cycle after oxidation. Solid curves and broken curves in (B) represent absolute part and imaginary part of the observed spectra, respectively.

2, but the curve fitting in the R space above 0.2 nm was not successful though all possible combinations among Mo−O, Mo−Al, Mo−Si, and Mo−Mo were examined within the permissible number of parameters. This may be due to the fact that not only single scattering by an atom located within 0.4 nm from Mo but also multiple scattering involving several atoms may contribute to the EXAFS oscillations. The EXAFS analysis for the Mo(1)/HY oxidized at 573 K revealed that the first shell contained two components and the feature near 0.4 nm was weak but still present.

EXAFS Simulation Using Feff 8.0. Simple curve fitting procedure for analysis of EXAFS oscillations was not appropriate because the backscattering by several kinds of atoms and the multiple scattering for various paths contribute to the oscillation. For conventional SiO_2 or Al_2O_3 supported catalysts the support surfaces are heterogeneous and the contributions of the scattering by atoms located at medium and large distances interfere with each other and become invisible in many cases. In this study the support is a crystalline material and the contributions by the atoms of the zeolite framework at long distances are visible in the EXAFS FT spectra (Figure 5).

TABLE 2: Pairs of Oxygen Atoms That Can Make Bonds with Mo and the Numbers of Lattice Points for Mo[a]

pairs of oxygen atoms	no. of lattice points possibly occupied by Mo	min value of R_f/%	no. of lattice points	
			R_f < 20%	R_f < 30%
O(A), O(F)	6848	10.4	849	2328
O(A), O(D)	0			
O(A), O(B)	1199	20.6	0	6
O(A), O(C)	1330	28.5	0	5
O(D), O(E)	2640	23.5	0	15
O(E), O(F)	2497	23.9	0	4
O(E), O(L)	0			
O(E), O(G)	9485	19.5	1	179
O(D), O(K)	0			
O(D), O(H)	1522	24.2	0	11
O(D), O(I)	10967	23.8	0	27
O(D), O(J)	2714	23.9	0	12
O(F), O(K)	1523	29.4	0	1

[a] Notation of oxygen atoms is indicated in Figure 1.

Therefore, simulation of the EXAFS oscillation with Feff 8.00 was performed using a known crystal structure of HY.

HY zeolite is classified as Faujasite zeolite, as depicted in Figure 5, where sodalite cages are bridged with hexagonal prisms. All the T sites (either Si or Al) consisting of the Faujasite type zeolite are equivalent locally, and there are only four kinds of oxygen atoms in the zeolite framework, as denoted by (a)−(d) in Figure 5. It was found by the analysis of the first shell that the Mo−O distance was 0.206 nm and the coordination number was 2. Thus Mo should have bondings with at least two oxygen atoms. The EXAFS analysis excluded the direct bonding such as Mo−Al, Mo−Si, and Mo−Mo. This is reasonable because Mo has a high affinity with oxygen atoms. Because Mo, Al, and Si atoms tend to be cationic in the zeolite framework, the repulsive Coulombic interaction between them seems to be operative and the distance between them is likely to be larger than 0.3 nm. The threshold value for this condition was taken as 0. 27 nm in the treatment described below for the more tolerant consideration. The space where Mo may be located was sought under the restrictions mentioned above.

First of all, all 13 pairs of oxygen atoms with an interatomic distance less than 0.5 nm were obtained as listed in Table 2. Mo is assumed to be located in the range 0.20−0.26 nm from these oxygen atoms and more than 0.27 nm away from all the T sites. Lattice points were produced on a three-dimensional grid of 0.005 nm within this space, resulting in 40 725 points. At each point Mo was placed and the nearest-neighbor oxygen atoms were displaced from the original points so that the Mo−O distance satisfied the observed 0.206 nm. Table 3 lists the displacement distances of the nearest neighbor oxygen atoms corresponding to each possible site for Mo where the lowest R_f value is obtained. Crystallographic data for HY zeolite were obtained from the ICSD database[29] for the zeolite with a similar Si/Al ratio.

TABLE 3: Displacement Distance of the Oxygen Atoms for the Cases with the Minimum R_f Value for Each Site[a]

site	oxygen atoms bonding with Mo	displacement distance/nm	R_f/%
$S_{I'}$	O(D)	0.032	23.8
	O(I)	0.032	
$S_{II'}$	O(E)	0.051	19.5
	O(G)	0.001	
S_{III}	O(F)	0.051	29.4
	O(K)	0.035	
$S_{III'}$	O(A)	0.043	10.4
	O(F)	0.051	

[a] Notation of oxygen atoms is indicated in Figure 1.

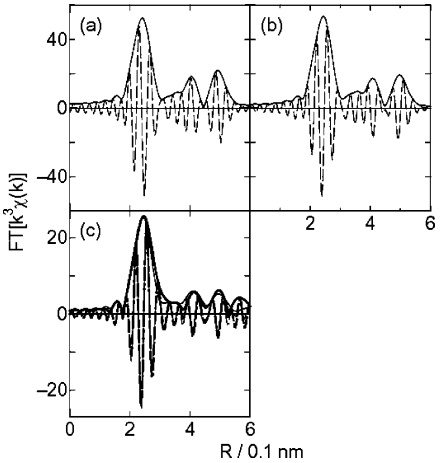

Figure 6. Fourier transforms of the k^3-weighted EXAFS oscillation of Mo foil: (a) Feff 8.0 simulation without SCF; (b) Feff 8.0 simulation with SCF; (c) observed results and Feff 8.0 simulation (Debye temperature = 450 K). Key: (thick solid line) absolute part of observed spectrum; (thick dashed line) imaginary part of observed spectrum; (thin solid line) absoulte part of calculated spectrum; (thin dashed line) imaginary part of calculated spectrum.

Treatment of the Debye−Waller factor is an important issue for the reproduction of EXAFS oscillations using Feff 8.0. The Debye−Waller factor relates to both the thermal disorder and the geometric disorder. In an ordinary EXAFS analysis, Debye−Waller factor is treated as a fitting parameter and obtained simultaneously with bond length and coordination number. The present Mo/HY system includes many scattering atoms, and about 100 atoms have to be taken into consideration for different multiple scattering paths even if the path length is confined below 0.6 nm. The maximum number of independent parameters (N_{ind}) permitted in the EXAFS analysis is given by the Nyquist equation as mentioned in the Experimental Section. In the case of Mo/HY, the R range was 0.1−0.42 nm and the k range was 30−120 nm^{-1} and N_{ind} is calculated to be 20.3. Therefore Debye−Waller factors cannot be fitted for all the multiple scattering paths. In this limited situation a Debye model would be convenient to evaluate Debye−Waller factors as a harmonic oscillator system, which is valid for isotropic monatomic lattice having only acoustic phonon branches. Though Mo/HY is not a monatomic lattice material and has optical phonon modes and hence does not satisfy the conditions for the Debye model strictly, we adopted this model because other reasonable and achievable methods are not available.

Reproduction of EXAFS functions using the Debye model and Feff 8.00 were examined for reference Mo compounds. Results for Mo foil are shown in Figure 6. Mo foil is a bcc monatomic lattice material and satisfies the demand for the Debye model. Parts a and b of Figure 6 correspond to the results

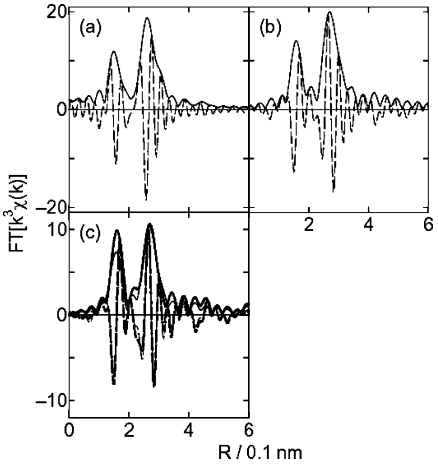

Figure 7. Fourier transforms of the k^3-weighted EXAFS oscillation of $Mo(CO)_6$: (a) Feff 8.0 simulation without SCF; (b) Feff 8.0 simulation with SCF; (c) observed results and Feff 8.0 simulation (Debye temperature = 1000 K). Key: (thick solid line) absolute part of observed spectrum; (thick dashed line) imaginary part of observed spectrum; (thin solid line) absoulte part of calculated spectrum; (thin dashed line) imaginary part of calculated spectrum.

without and with the SCF option, respectively. The former was calculated in less than 1 min and the latter needed about 20 min. It took about 1 h for other reference Mo compounds. Though calculation needs a longer time, the inclusion of the SCF option can unify the Fermi energy for all atoms, resulting in an obviously better agreement between calculated and experimental results of Fourier transformed EXAFS functions. Figure 6c was obtained by setting the Debye temperature of 450 K and the measurement temperature of 300 K in the Feff 8.0 simulation, which could reproduce the experimental results well. The Debye temperature for the Mo foil was also found to be 450 K by the measurement of the specific heat at the low-temperature limit and fitting to the Debye T^3 law.

Similar procedures were done for other multi-atom lattice materials and the inclusion of SCF was found to be more effective than the case for Mo foil. Figure 7a shows the results for $Mo(CO)_6$, where the experimental results were reproduced well by setting the Debye temperature at 1000 K. The contribution of the first shell (Mo−C) was a little underestimated by the Debye model. This is because the Debye−Waller factor was overestimated for the direct chemical bonding of Mo−C. Figure 8 shows the results for $Mo_2(CH_3COO)_4$. In this case the use of Debye temperature of 1000 K was enough to reproduce the experimental results. This compound has an Mo−O bond with a length of 0.214 nm and an Mo−Mo bond with a length of 0.210 nm. Figure 9 shows the simulation results for MoO_2. Because MoO_2 has a low symmetry, curve-fitting shell analysis was not possible. Assuming the Debye model and a Debye temperature of 500 K with the SCF option in Feff 8.0 simulation, good agreement with the observed results except the first shell was obtained. As to MoO_3 the Feff 8.0 calculation could not reproduce the observed results (not shown) probably because MoO_3 is a layer compound and the Debye model is inappropriate, in this case due to its strong anisotropy. As to Na_2MoO_4 the Debye model with a Debye temperature of 600 K could reproduce a small feature at 0.35 nm in the observed Fourier transformed spectrum though the intensity of the first shell is deviated, as shown in Figure 10.

In this way the Feff 8.0 calculations with the Debye model could reproduce the observed spectra for $Mo(CO)_6$, $Mo_2(CH_3COO)_4$, MoO_2, and Na_2MoO_4, except for MoO_3, and it was found that the Debye−Waller factor for the first shell corre-

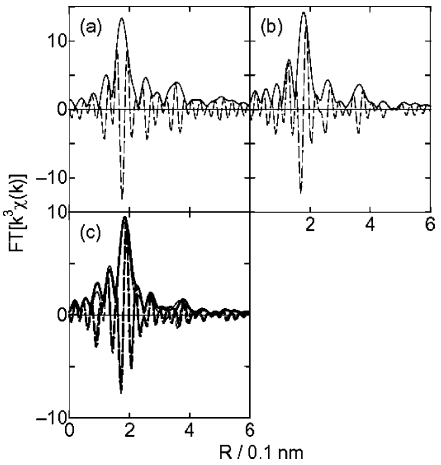

Figure 8. Fourier transforms of the k^3-weighted EXAFS oscillation of $Mo_2(CH_3CO_2)_4$: (a) Feff 8.0 simulation without SCF; (b) Feff 8.0 simulation with SCF; (c) observed results and Feff 8.0 simulation (Debye temperature = 1000 K). Key: (thick solid line) absolute part of observed spectrum; (thick dashed line) imaginary part of observed spectrum; (thin solid line) absoulte part of calculated spectrum; (thin dashed line) imaginary part of calculated spectrum.

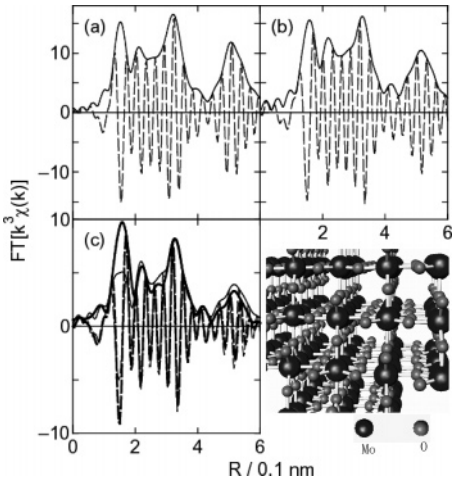

Figure 9. Fourier transforms of the k^3-weighted EXAFS oscillation of MoO_2: (a) Feff 8.0 simulation without SCF; (b) Feff 8.0 simulation with SCF; (c) observed results and Feff 8.0 simulation (Debye temperature = 500 K). The structure of MoO_2 is also shown. Key: (thick solid line) absolute part of observed spectrum; (thick dashed line) imaginary part of observed spectrum; (thin solid line) absoulte part of calculated spectrum; (thin dashed line) imaginary part of calculated spectrum.

sponding to a direct chemical bond should be estimated in a different way. These examples show that the Debye model can be a fairly good model for the materials that do not satisfy the demands for the Debye model rigidly. Hence, we have applied the Debye model to the structural analysis of Mo/HY.

Feff 8.0 Simulation for Mo/HY. As described above, the inclusion of the SCF option needs about 1 h for each set of coordinates. Therefore it is not practical to calculate all the 40 725 cases including the SCF option. As shown in Figure 11, the non-SCF calculation with the correction of energy level of Mo by 7.0 eV gave almost the same results as the SCF calculation. This procedure was adopted for the Feff 8.0 simulation to conduct the first screening. The production of coordinates, the Feff simulation, and R_f calculation were regulated automatically by a macro program. Table 2 lists the minimum value of R_f (reliable factor), the number of points with R_f below 20%, and that below 30% versus oxygen atom pairs.

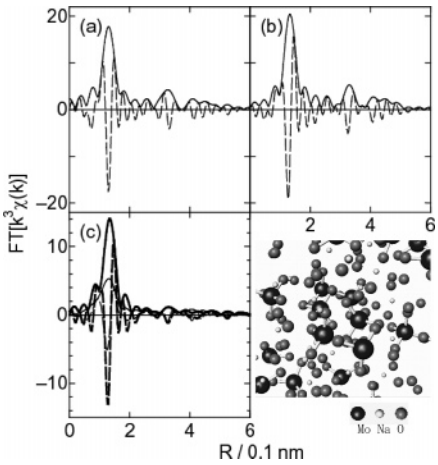

Figure 10. Fourier transforms of the k^3-weighted EXAFS oscillation of Na_2MoO_4: (a) Feff 8.0 simulation without SCF; (b) Feff 8.0 simulation with SCF; (c) observed results and Feff 8.0 simulation (Debye temperature = 600 K). The structure of Na_2MoO_4 is also shown. Key: (thick solid line) absolute part of observed spectrum; (thick dashed line) imaginary part of observed spectrum; (thin solid line) absoulte part of calculated spectrum; (thin dashed line) imaginary part of calculated spectrum.

Table 2 clearly shows that the pair of O(A) and O(F) gave many good possibilities for Mo location compared to other pairs, suggesting that Mo favors bonds with O(A) and O(F). The calculations including the SCF option were done for Mo atoms making bonds with O(A) and O(F). Several other pairs with relatively low R_f values were also calculated in a similar way as a comparison. Some representative results are described below. The calculated results corresponding to S_I', S_{II}, S_{III}, and S_{III}' sites were shown in Figures 12−15, where the Debye temperature was fixed at 600 K. The best result was obtained for the S_{III}' site (Figure 15). For this model, the Debye temperature and the Debye−Waller factor for the first shell were allowed to vary in the fitting process and the obtained best fitting is shown in Figure 16. The Debye temperature was found to be (700 ± 100) K.

The Mo(1)/HY oxidized under the mild condition was also analyzed by EXAFS as shown in Figure 17. It was found by the curve fitting analysis that a Mo atom is bonded with two oxygen atoms at a distance of 0.171 nm and with two other oxygen atoms at a distance of 0.202 nm. Two oxygen atoms were added to the S_{III}' model so that Mo has a tetrahedral symmetry with Mo−O bond distances satisfying the curve fitting analysis. The observed EXAFS functions were reproduced well with an R_f value of 3.85% by a FEFF 8.0 simulation with a Debye temperature of (640 ± 80) K. In this model the Mo site is displaced by 0.06 nm as compared to the original S_{III}' position.

DFT Calculations. To confirm the proposed structures obtained by the EXAFS analysis, DFT calculations were performed. The calculations were performed with a cluster model. The FAU model with Si/Al = 1 was obtained from the database (Cerius Interface). Two neighboring four-membered rings were cut out and terminated with OH group to model the S_{III}' site. This model was optimized with a confinement in which Si, Al, and oxygen atoms were fixed and terminal hydrogen atoms were allowed to move. The resultant structure is shown in Figure 18a. To model Mo(1)/HY at the S_{III}' site, H(1) was removed and Mo was coordinated with O(1) and O(2), resulting in the formal charge of Mo cation being unity. The positions of Mo, O(1), and O(2) and terminal hydrogens were optimized as shown in Figure 18b. The model for the mildly oxidized Mo(1)/HY was obtained by adding two oxygen atoms on the

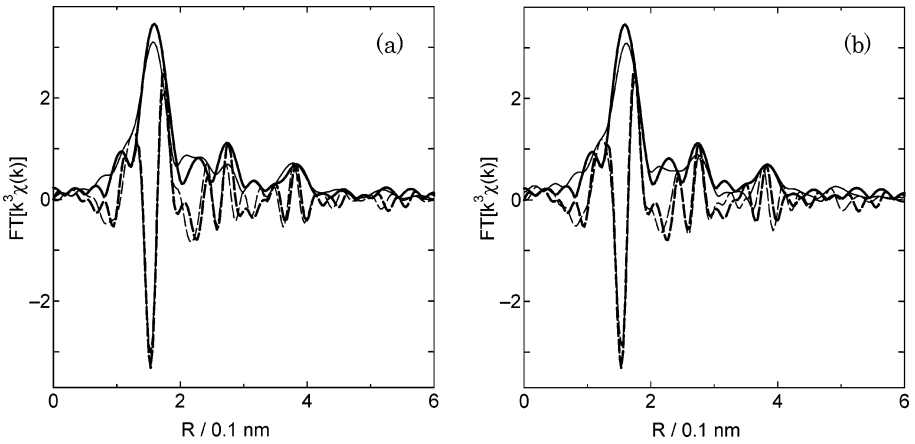

Figure 11. Observed Fourier transformed EXAFS spectra and calculated Fourier transformed EXAFS spectrum using Feff 8.0 without SCF (a) and with SCF (b). The thick solid curve and thick broken curve represent absolute and imaginary parts of the observed spectrum, respectively. The thin solid curve and thin broken curve represent absolute and imaginary part of the calculated spectrum, respectively.

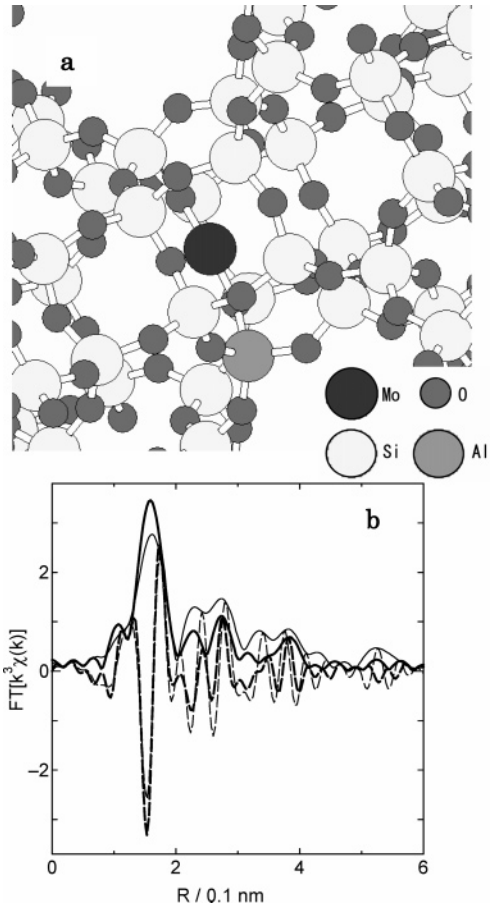

Figure 12. (a) Representative structure of Mo/HY near S_I'. (b) Fourier transforms of the k^3-weighted EXAFS oscillation of the observed spectrum and the calculated spectrum using Feff 8.0. Key: (thick solid line) absolute part of observed spectrum; (thick dashed line) imaginary part of observed spectrum; (thin solid line) absoulte part of calculated spectrum; (thin dashed line) imaginary part of calculated spectrum.

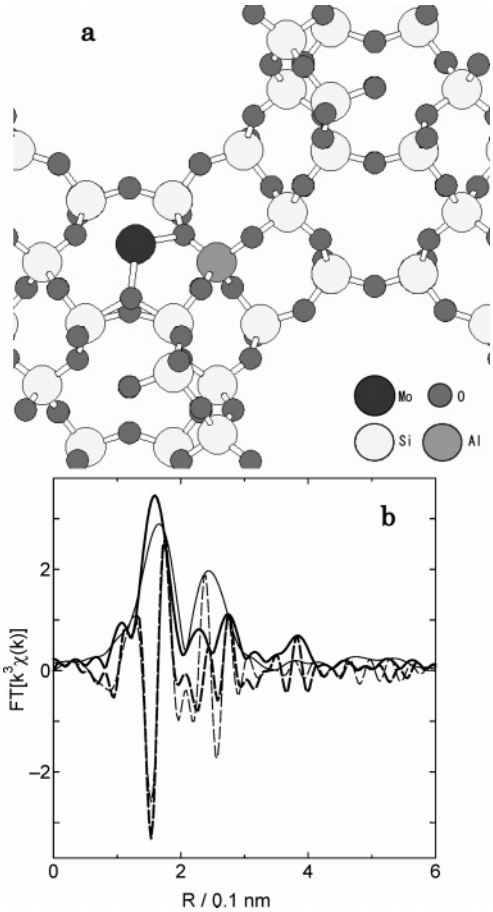

Figure 13. (a) Representative structure of Mo/HY near S_{II}'. (b) Fourier transforms of the k^3-weighted EXAFS oscillation of the observed spectrum and the calculated spectrum using Feff 8.0. Key: (thick solid line) absolute part of observed spectrum; (thick dashed line) imaginary part of observed spectrum; (thin solid line) absoulte part of calculated spectrum; (thin dashed line) imaginary part of calculated spectrum.

Mo atom, and optimization was performed under the condition that Mo and the neighboring four oxygen atoms were allowed to move. The optimized structure is shown in Figure 18c. Table 4 compares the interatomic distances between Mo and other atoms obtained by the EXAFS analysis and the DFT calculations. Table 4 indicates that the model obtained by the EXAFS analysis is reasonable in the sense that the DFT calculation is in agreement with the model at least locally optimized.

Discussion

The location of cations in Faujasite (FAU)-type zeolites have been extensively studied and summarized in Figure 1.[30−32] Energetically favorable sites are S_I in a hexagonal prism or S_I' coordinated by a six-membered ring. The next favorable sites are S_{II}, which is positioned in a supercage and coordinated with three oxygen atoms from a six-membered window of the sodalite cage, or S_{II}', which is displaced by about 0.05 nm inside the

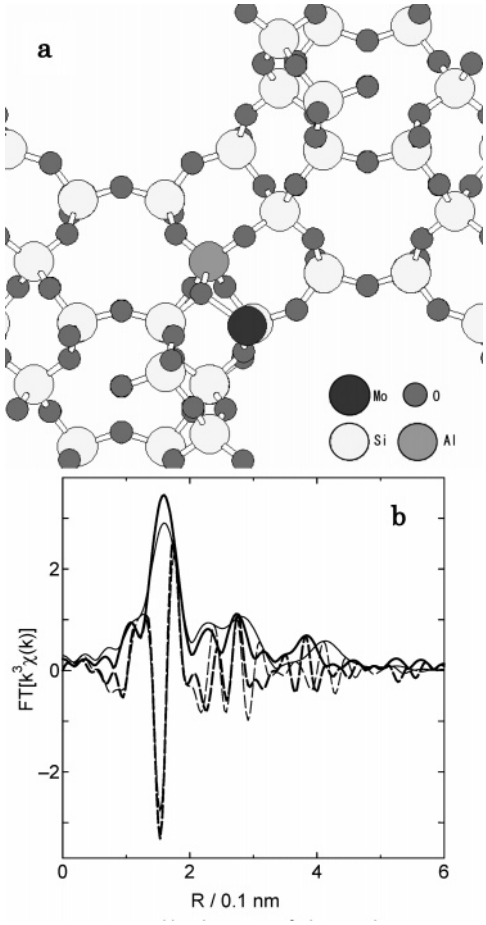

Figure 14. (a) Representative structure of Mo/HY near S_{III}. (b) Fourier transforms of the k^3-weighted EXAFS oscillation of the observed spectrum and the calculated spectrum using Feff 8.0. Key: (thick solid line) absolute part of observed spectrum; (thick dashed line) imaginary part of observed spectrum; (thin solid line) absoulte part of calculated spectrum; (thin dashed line) imaginary part of calculated spectrum.

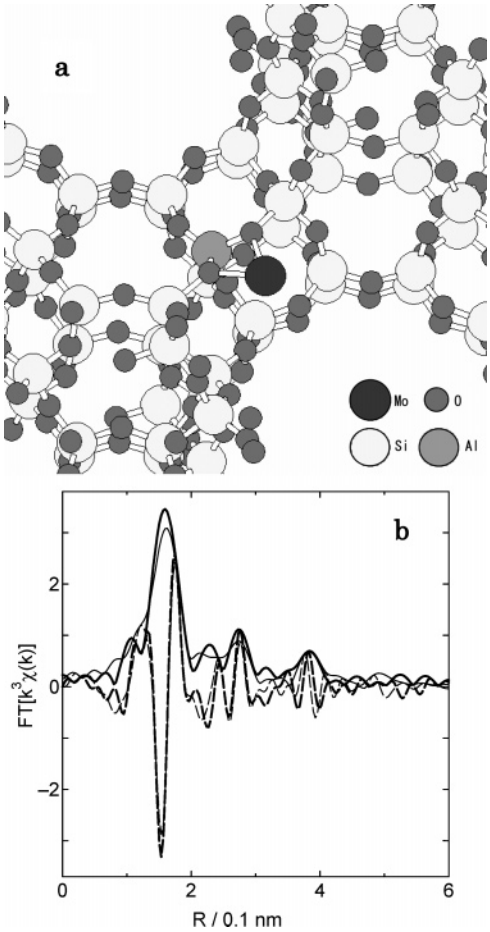

Figure 15. (a) Representative structure of Mo/HY near S_{III}'. (b) Fourier transforms of the k^3-weighted EXAFS oscillation of the observed spectrum and the calculated spectrum using Feff 8.0. Key: (thick solid line) absolute part of observed spectrum; (thick dashed line) imaginary part of observed spectrum; (thin solid line) absoulte part of calculated spectrum; (thin dashed line) imaginary part of calculated spectrum.

sodalite cage from S_{II}. In the case of a small number of cations these sites are enough to allocate cations, but the number of cations becomes larger than the number of S_{II} sites, and energetically unfavorable sites such as S_{III} and S_{III}' are occupied partially.[31] The S_{III} site is located at a four-membered ring of the sodalite cage and the S_{III}' site is located at the boundary of the sodalite cage and the hexagonal prism. Cations are coordinated by three oxygen atoms at S_I, S_I', S_{II}, and S_{II}'. The cation at the S_{III} site is coordinated by two oxygen atoms and that at S_{III}' is coordinated by four oxygen atoms, two of which are rather distant from the cation.

The position of Mo cations for the Mo/HY prepared by the adsorption−decomposition method in this study was found to be close to the S_{III}' site by the Feff 8.0 simulation. This site is less favorable energetically, and there has been no report of the occupation of this site for Mo when the other sites are vacant. The reason for the preferential occupation of this site by Mo is explained as follows. In the HY sample before the CVD process the same number of protons as for Al exist as countercations, as observed by the OH stretching peaks in the FT-IR spectra (Figure 3). The protons in the HY zeolite exist at two kinds of positions on the oxygen atoms bonding to Al by neutron diffraction.[33] In the major case protons exist in a supercage and make bonds with the oxygen atom (A) on the side of the hexagonal prism connecting the sodalite cages (Figure 1), and in the minor case protons make bonds with the oxygen atom (B) on the boundary of the sodalite cage and the hexagonal prism (Figure 1). The former and the latter are assigned to the ∼3680 cm^{-1} peak and the ∼3600 cm^{-1} peak, respectively. A small peak at 3740 cm^{-1} in Figure 3 is assigned to silanols on the exterior surface of zeolite crystal. The proton bonding with the O(A) atom (OH group) exists in a supercage, where Mo-$(CO)_6$ is located after CVD. Because simultaneous desorptions of CO and H_2 were found in the TPD spectra for $Mo(CO)_6$/HY (Figure 3), Mo atoms are considered to be attached on the HY framework by the decarbonylation of $Mo(CO)_6$ accompanied with the reaction with the protons on the O(A) atoms. The Mo cation at the S_{III}' site makes bonds with two oxygen atoms, one of which bonded with the proton before CVD. When Eu^{3+} was introduced in the Y zeolite by ion exchange, Eu^{3+} was first located at the S_{II} site and migrated to the S_I' site below 473 K.[34] The decarbonylation temperature (450 K) for $Mo(CO)_6$/HY is close to this example, suggesting a possible migration to the S_I or S_{II} sites, but it is not the case.

The discussion based on the number of sites is useful. In a supercage there are two S_I sites, four S_I' sites, four S_{II}' sites, and six S_{III}' sites. Mo is homogeneously attached on the HY zeolite up to six atoms per supercage, as suggested by the data in Figures 2 and 3. If S_I, S_I', or S_{II}' sites are involved in the Mo attachment, a single kind of the sites cannot accommodate six Mo atoms in a supercage, resulting in heterogeneous occupation of several kinds of sites. If there is a difference in stabilization energy for the Mo bonding among the different sites, energetically favorable sites should be preferentially occupied, which

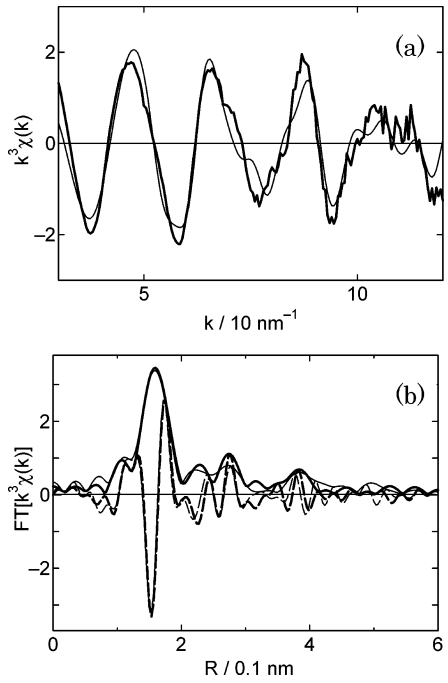

Figure 16. k^3-weighted EXAFS oscillation (a) and Fourier transforms (b) of the observed spectrum for the Mo(1)/HY (thick curves) and the Feff 8.0 simulation (thin curves) corresponding to the occupation of S_{III}'. R_f is 6.86%.

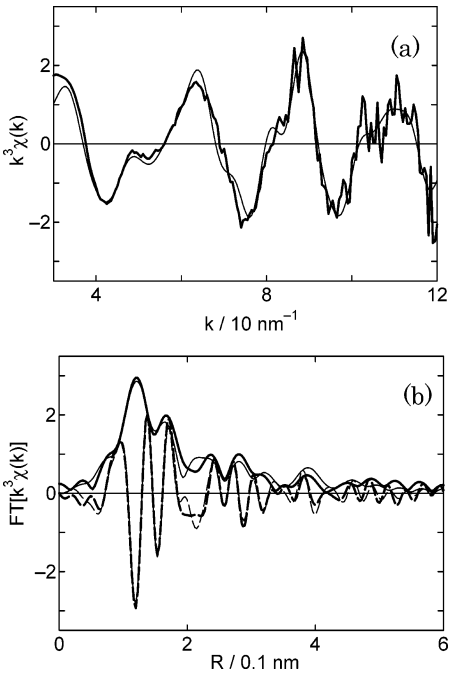

Figure 17. k^3-weighted EXAFS oscillation (a) and Fourier transforms (b) of the observed spectrum for the Mo(1)/HY oxidized under the mild condition (thick curves) and the Feff 8.0 simulation (thin curves). Key: (thick solid line) absolute part of observed spectrum; (thick dashed line) imaginary part of observed spectrum; (thin solid line) absoulte part of calculated spectrum; (thin dashed line) imaginary part of calculated spectrum. R_f is 3.85%.

causes a coverage dependence on the spectra. If a difference in energy is small and two kinds of sites are occupied with a certain relative ratio, a coverage dependence would appear. These are not in agreement with the present results.

On the other hand, the S_{III}' site is indirectly supported by the fact that there are six S_{III}' sites in a supercage as well as the fact that protons are originally bonded to the S_{III}' sites. Although

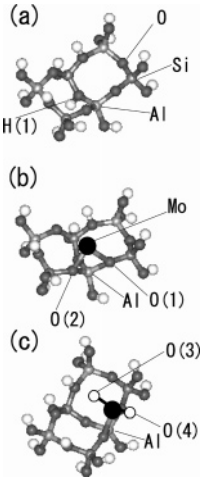

Figure 18. Optimized structures obtained by DFT calculations: (a) $Si_3Al_3O_{17}H_{13}$; (b) $MoSi_3Al_3O_{17}H_{12}$; (c) $MoSi_3Al_3O_{19}H_{12}$.

TABLE 4: Interatomic Distances Obtained by EXAFS Analysis and DFT Calculations

		Mo−O/nm	Mo═O/nm	Mo−Al/nm	Mo−Si/nm
Mo(1)/HY	EXAFS	0.208, 0.211		0.299	0.366, 0.358
	DFT	0.217, 0.220		0.285	0.366, 0.346
oxidized	EXAFS	0.202, 0.202	0.171, 0.171	0.294	0.350, 0.363
Mo(1)/HY	DFT	0.217, 0.215	0.172, 0.173	0.290	0.353, 0.363

there are six S_{III} sites in a supercage, this possibility is excluded because the simulated result for S_{III} is different from the observed data, as shown in Figure 14 and the position of S_{III} is far from the position of inherent proton.

In the simulation of EXAFS function the Debye model was used to estimate Debye−Waller factor though the present samples do not strictly satisfy the requirements for the Debye model. Several examples have been reported for the simulation of EXAFS functions using the Debye model. Experimental data for Cu foil were reproduced by the Feff 8.0 simulation with the Debye model, which is suitable for the model.[35] Reproduction of the experimental results by the Feff 8.0 simulation with the Debye model was also reported for GaN doped with Mg and Si, which does not satisfy the requirements for the Debye model.[36] Thus the Debye model is also a good approximation for materials deviating from the original assumption to account for the Debye−Waller factor. The parameters used in the Feff 8.0 simulation for Mo/HY were coordinates (x, y, z) of the Mo atom, two sets of (distance of displacement and Debye−Waller factor) for two oxygen atoms bonding with the Mo atom, and ΔE_0. The number of the parameters are substantially smaller than the allowable maximum number of parameters, 19.

The distance of the displacement of zeolite oxygen atoms by the introduction of Mo atom is discussed here. Usually, introduction of cations in zeolite results in distortion of the zeolite framework and oxygen atoms in the framework are displaced by about 0.03 nm.[37] In this study the distance of the displacement of oxygen atoms due to the Mo attachment was found to be about 0.05 nm. As a result, the bond distance of Al−O was elongated to 0.168 and 0.177 nm, and that of the Si−O bond was elongated to 0.190 and 0.198 nm. The Al−O bond distance in HY is 0.165 nm. As for γ-Al_2O_3 the Al−O bond distance of tetrahedron is 0.185 nm and that of the octahedron is 0.194 nm. Judging from these values, the elongated Al−O distances in the Mo/HY are within a reasonable range and the Al−O bond is still strong. However, the observed Si−O distances are rather abnormally long. Dehydration of brewsterite single crystal by annealing under vacuum causes

the scission of T−O-T bond and the T−O bond is elongated to be 0.2 nm.[38−40] Hence, the present long Si−O bond distance can be interpreted as a quasi-disruption of Si−O bond by the formation of covalent Mo−O bond accompanied with charge redistribution as follows.

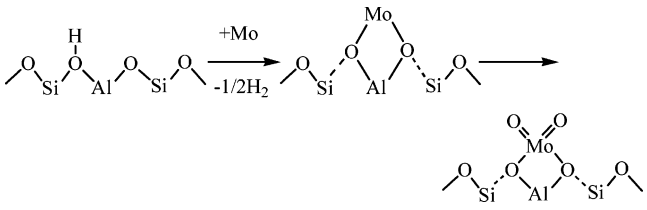

Mild oxidation of Mo on the S_{III}' site without destruction of the zeolite framework occurs by exposure of Mo/HY to 1 equiv amount of oxygen and subsequent annealing. In the EXAFS spectrum of this sample in the *R* space the long-distance peak at 0.4 nm was weakened but still observable. The simulation using Feff 8.0 could reproduce the observed EXAFS function. The proposed structure is shown in Figure 15, where the position of Mo is displaced by 0.06 nm as compared to the position in the Mo/HY in the direction to reduce the distortion of the zeolite framework. The Mo atom coordinated by the two oxygen atoms is unstable because of the unsaturated coordination, and the large distortion in the zeolite framework is induced as shown in the above scheme. The distortion is relaxed by the mild oxidation forming two additional Mo═O bonds at 0.171 nm.

Only a preceding result similar to the present one was reported for rhodium dicarbonyls in a highly dealuminated Y zeolite by Goellner et al. [41] They claimed that Rh was located at the boundary of a four-membered ring of hexagonal prism and a six-membered ring of sodalite cage. In the present study Mo was found to be located at the boundary of a four-membered ring of hexagonal prism and a four-membered ring of sodalite cage as shown in Figure 15. The site occupation for the Rh atoms in the Y zeolite was not directly determined from the EXAFS experimental results but demonstrated by the comparison of stabilized energies obtained by DFT calculations.[41] Therefore the present study is the first example that the position of cations in zeolite was determined by EXAFS.

Conclusion

Introduction of $Mo(CO)_6$ in HY zeolite by a CVD method and subsequent decarbonylation resulted in the attachment of two Mo atoms per supercage every CVD-decarbonylation cycle up to six Mo atoms after three cycles. One equivalent amount of protons in HY zeolite to the Mo quantity was consumed in the attachment of Mo, evolving H_2, accompanied with the formation of Mo−O bonds. There existed several definite peaks in Fourier transformed EXAFS functions for the Mo/HY in the *R* range 0.1−0.5 nm, but these contributions could not be analyzed by a usual curve fitting technique because of many possible multiple scattering paths in the HY zeolite crystalline framework. The EXAFS analysis including multiple scattering based on Feff 8.0 calculations with the Debye model revealed that the Mo atom was attached on S_{III}' site in a bidentate form

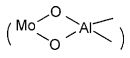

The zeolite framework was significantly distorted by the introduction of Mo, where two Si−O bonds adjacent to the Al atom connecting to the Mo atom were disrupted, resulting in protrusion of the

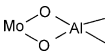

unit from the zeolite framework. In the mild oxidation of the low-valent Mo/HY two Mo═O bonds were formed in addition to the two Mo−O bonds and the position of Mo was displaced to relieve the distortion of zeolite framework. The location of Mo cations on the S_{III}' sites in HY was determined by the detailed EXAFS analysis for the first time. The DFT calculation confirmed the local structure around Mo.

Acknowledgment. We thank Dr. T. Shido for his help in measurements of a part of the EXAFS spectra. This study was supported by a Grant-in-aid for The 21st Century COE Program for Frontiers in Fundamental Chemistry from the Ministry of Education, Culture, Sports, Science and Technology. XAFS measurements were carried out with the approval of the Photon Factory Advisory Committee (PAC) (proposal no. 2001G098).

References and Notes

(1) Iwasawa, Y. *Adv. Catal.* **1987**, *35*, 187.
(2) Iwasawa, Y. *Catal. Today* **1993**, *18*, 21.
(3) Iwasawa, Y. *Stud. Surf. Sci. Catal.* **1996**, *101*, 21.
(4) Thomas, J. M.; Thomas, W. J. *Principles and Practice of Heterogeneous Catalysis*; VCH: Weinheim, 1997.
(5) Iwasawa, Y. *Tailored Metal Catalysts*, Reidel: Dordrecht, 1986.
(6) Montovani, E.; Palladirio, N.; Zanotti, A. *J. Mol. Catal.* **1977/1978**, *3*, 385.
(7) Ichikawa, M. *Adv. Catal.* **1992**, *38*, 283.
(8) Kozlov, A.; Asakura, K.; Iwasawa, Y. *Chem. Lett.* **1997**, 313.
(9) Kozlov, A.; Asakura, K.; Iwasawa, Y. *J. Chem. Soc., Faraday Trans.* **1998**, *94*, 809.
(10) McCarthy, T. J.; Marques, C. M. P.; Trevino, H.; Sachtler, W. M. H. *Catal. Lett.* **1997**, *43*, 11.
(11) Okamoto, Y.; Maezawa, A.; Kane, H.; Mitsushima, I.; Imanaka, T. *J. Chem. Soc., Faraday Trans. 1* **1988**, *84*, 851.
(12) Okamoto, Y.; Kane, H.; Imanaka, T. *Chem. Lett.* **1988**, 2005.
(13) Abdo, S.; Howe, R. F. *J. Phys. Chem.* **1983**, *87*, 1713.
(14) Ozkar, S.; Ozin, G. A.; Moller, K.; Bein, T. *J. Am. Chem. Soc.* **1990**, *112*, 9575.
(15) You-Sing, Y.; Howe, R. F. *J. Chem. Soc., Faraday Trans. 1* **1986**, *82*, 2887.
(16) Asakura, K.; Noguchi, Y.; Iwasawa, Y. *J. Phys. Chem. B* **1999**, *103*, 1051.
(17) Okamoto, Y.; Imanaka, T.; Asakura, K.; Iwasawa, Y. *J. Phys. Chem.* **1991**, *95*, 3700.
(18) Yamaguchi, A.; Suzuki, A.; Shido, T.; Inada, Y.; Asakura, K.; Nomura, M.; Iwasawa, Y. *Catal. Lett.* **2001**, *71*, 203.
(19) Yamaguchi, A.; Suzuki, A.; Shido, T.; Inada, Y.; Asakura, K.; Nomura, M.; Iwasawa, Y. *J. Phys. Chem. B* **2002**, *106*, 2415.
(20) Maezawa, A.; Kane, H.; Okamoto, Y.; Imanaka, T. *Chem. Lett.* **1988**, 241.
(21) Okamoto, Y.; Maezawa, A.; Kane, H.; Imanaka, T. *J. Catal.* **1988**, *112*, 585.
(22) Abdo, S.; Howe, R. F. *J. Phys. Chem.* **1983**, *87*, 1722.
(23) Shido, T.; Asakura, K.; Noguchi, Y.; Iwasawa, Y. *Appl. Catal. A-Gen.* **2000**, *194*, 365.
(24) Stern, E. A.; Newville, M.; Ravel, B.; Yacoby, Y.; Haskel, D. *Phys. B* **1995**, *208*, 117.
(25) Stern, E. A. *Phys. Rev. B* **1993**, *48*, 9825.
(26) Ankudinov, A. L.; Ravel, B.; Rehr, J.; Conradson, S. D. *Phys. Rev. B* **1998**, *58*, 7565.
(27) Delly, B. *J. Chem. Phys.* **1990**, *92*, 508.
(28) Perdew, J. P.; Wang, Y. *Phys. Rev. B* **1992**, *45*, 13244.
(29) *Inorganic Crystal Database (ICSD)*; FIZ Karlsruhe NIST, 2003.
(30) Jaramillo, E.; Auerbach, S. *J. Phys. Chem. B* **1999**, *103*, 9589.
(31) Vitale, G.; Mellot, C.; Bull, L.; Cheetham, A. *J. Phys. Chem. B* **1997**, *101*, 4559.
(32) Marra, G.; Fitch, A.; Zecchina, A.; Ricchiardi, G.; Salvalaggio, M. *J. Phys. Chem. B* **1997**, *101*, 10653.
(33) Czjzek, M.; Jobic, H.; Fitch, A.; Vogt, T. *J. Phys. Chem.* **1992**, *96*, 1535.
(34) Berry, F. J.; Carbucicchio, M.; Chiari, A.; Johnson, C.; Moore, E. A. *J. Mater. Chem.* **2000**, *10*, 2131.
(35) Rehr, J. J.; Albers, R. C. *Rev. Mod. Phys.* **2000**, *72*, 621.
(36) Katsikini, M.; Moustakas, T. D.; Paloura, E. C. *J. Synchrot. Radiat.* **1999**, *6*, 555.

(37) Pierloot, K.; Delabie, A.; Ribbing, C.; Verberckmoes, A. A.; Schoonheydt, R. A. *J. Phys. Chem. B* **1998**, *102*, 10789.
(38) Alberti, A.; Vezzalini, G.; Quartieri, S.; Cruciani, G.; Bordiga, S. *Microporous Mesoporous Mater.* **2001**, *42*, 277.
(39) Sacerdoti, M.; Vezzalinni, G.; Quartieri, S. *Microporous Mesoporous Mater.* **2000**, *41*, 107.
(40) Alberti, A.; Sacerdoti, M.; Quartieri, S.; Vezzalini, G. *Phys. Chem. Miner.* **1999**, *26*, 181.
(41) Goellner, J.; Gates, B. C.; Vayssilov, G.; Rosch, N. *J. Am. Chem. Soc.* **2000**, *122*, 8056.